Fluid dynamics and wave-structure interactions

Göteman, Malin
Uppsala University

Mayon, Robert
Dalian University of Technology

Liu, Yingyi
Research Institute for Applied Mechanics, Kyushu University

Zheng, Siming
University of Plymouth

他

https://hdl.handle.net/2324/4798342

KYUSHU UNIVERSITY

Fluid dynamics and wave-structure interactions

Malin Göteman[1], Robert Mayon[2], Yingyi Liu[3],
Siming Zheng[4], Rongquan Wang[2]
[1]Uppsala University, malin.goteman@angstrom.uu.se,
[2]Dalian University of Technology, rmayon@dlut.edu.cn,
[3]Kyushu University, liuyingyi@riam.kyushu-u.ac.jp,
[4]University of Plymouth, siming.zheng@plymouth.ac.uk

2.1 FLUIDS AND WAVE-STRUCTURE INTERACTIONS

To understand the energy absorption from ocean waves, it is necessary to understand the source itself – the fluid and the ocean waves – and how it interacts with structures, such as a wave energy converter. Here, the properties and description of ocean waves will first be discussed based on fundamental as well as stochastic principles, after which the hydrodynamic forces due to the waves and their interaction with bodies in the fluid will be discussed.

2.1.1 Ocean waves

Several types of ocean waves exist. Tsunami waves are very long, fast waves caused by an earthquake or landslide, and capillary waves are small ripples on the water surface, generated by the wind and dominated by surface tension effects. In wave energy applications, the waves of interest are *wind-generated gravity surface waves*, i.e., waves resulting from wind blowing at the ocean surface, and dominated by gravity and inertial forces. Wind-generated ocean waves are thus a renewable energy source, distilled in two steps from the solar energy incident on the earth, which causes wind and in the next step waves. As such, ocean waves contain more energy per unit volume than wind and solar energy, and the wave energy resource roughly resembles the characteristics of wind energy and is largest at high latitudes, as shown in Figure 1.24.

Figure 2.1: In general, ocean waves consist of waves of many frequencies, travelling simultaneously in different directions (left). Due to the dispersive property of ocean waves, waves propagating over long distances separate according to frequency, producing swells (right).

As water waves, ocean waves can in their most fundamental form be described by the Navier-Stokes equations for incompressible fluids, as will be discussed in Section 2.1.1.1. Numerical solutions of these equations form the basis for the computational fluid dynamics methods that are discussed in detail in Section 2.3. For many applications, however, simplified theories based on neglecting viscosity, turbulence, and non-linear effects of the fluid can be used, resulting in linear potential flow theory. These assumptions and their limits of validity will be discussed in Section 2.1.1.2. As we will see, the solutions describe surface waves that satisfy the *dispersion relation*, meaning that the waves are dispersive and travel with speeds proportional to their wave lengths. This gives rise to the formation of swells, which can be seen in Figure 2.1 and will be discussed in more detail in Section 2.1.1.3. From the linearity of the problem, a sum of solutions is again a solution to the linear potential flow theory, and ocean waves can, to a good approximation, be described as superpositions of sinusoidal waves with different frequencies and phases. Such irregular waves can be described by stochastical parameters and wave spectra, to be introduced in Section 2.1.1.4.

2.1.1.1 Navier-Stokes equations

The fundamental equations describing fluids are the Navier-Stokes equations together with the continuity equation. The continuity equation stems from the physical principle that the mass of the fluid element must be conserved, and can be expressed as:

$$\frac{\partial \rho}{\partial t} + \nabla \cdot (\rho \mathbf{u}) = 0 \tag{2.1}$$

where the first term represents the change in fluid density ρ and the second term the mass flow, and $\mathbf{u}$ denotes the fluid velocity.

Water can (to a good approximation) be considered incompressible [242], and to distinguish water from other fluids such as gases, an incompressibility constraint can

be imposed,

$$\nabla \cdot \mathbf{u} = 0. \tag{2.2}$$

Finally, the Navier-Stokes equation is derived from the fundamental principle of momentum conservation. In other words, it is derived by applying Newton's second law

$$\mathbf{F} = m\mathbf{a} \tag{2.3}$$

to a small fluid volume, and expressing on the left-hand-side all the forces acting on the fluid element, and expressing the right-hand-side as the density of the fluid times its acceleration, integrated over the fluid volume. The forces acting on the fluid are external forces (usually only gravity) and internal forces acting on the surface of the fluid element by neighbouring fluid elements. The internal force is called stress force and can be divided into pressure p (acting perpendicular to the surface) and shear stress (acting parallel). For incompressible fluids, the shear stress can be rewritten in terms of viscosity ν, and the Navier-Stokes equation takes the form

$$\frac{\partial \mathbf{u}}{\partial t} + \mathbf{u} \cdot \nabla \mathbf{u} = -\frac{1}{\rho}\nabla p + \nu \nabla^2 \mathbf{u} + \frac{1}{\rho}\mathbf{F}_{\text{ext}} \tag{2.4}$$

where $\mathbf{F}_{\text{ext}}$ is the external net force acting on the fluid, usually only the gravity force $\mathbf{F}_{\text{ext}} = \nabla(-\rho g z)$. For inviscid flow, the Navier-Stokes equations reduce to the Euler equations.

An incompressible fluid is thus governed by the continuity Eq. (2.1), an incompressibility constraint (2.2), and the Navier-Stokes Eq. (2.4). These form a system of non-linear partial differential equations, and finding analytical solutions is difficult, or impossible. In fact, to prove the existence of smooth solutions in three dimensions is one of the most important open problems in mathematics and physics, and a reward of 1 million USD has been offered by the Clay Mathematics Institute for a solution or counterexample.

To find solutions, there are two main approaches. The first, which will be discussed in detail in Section 2.3, is to discretise the problem and solve it using approximate numerical methods, such as Reynolds-averaged Navier-Stokes (RANS) computational fluid dynamics (CFD) methods. The second approach is to make assumptions to simplify the equations, such that analytical or numerical solutions can be readily found. This approach will now be discussed in detail in the remainder of this section and in Section 2.2.2.

2.1.1.2 Linear potential flow theory

Consider a fluid which is irrotational ($\nabla \times \mathbf{u} = 0$). This assumption is equivalent (at least for simply connected domains) to the fluid velocity being conservative, i.e., it is the gradient of some fluid velocity potential, $\mathbf{u} = \nabla\Phi$. Together with the incompressibility constraint in Eq. (2.2), this implies that the fluid potential satisfies the Laplace equation,
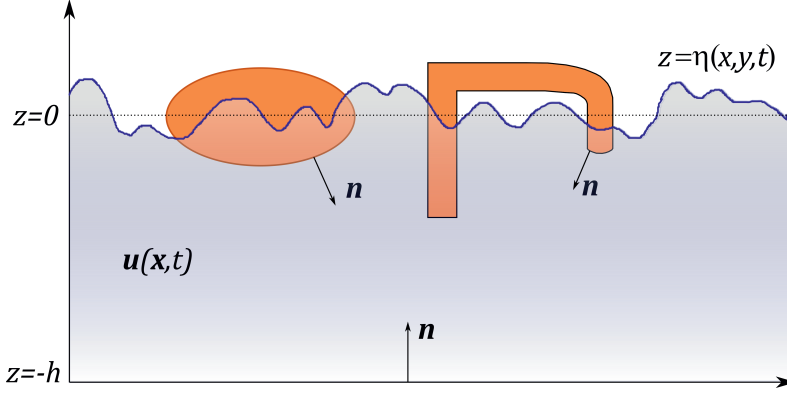
$$\nabla^2 \Phi = 0. \tag{2.5}$$

Figure 2.2: Notation of the fluid domain.

Furthermore, assume that the fluid is ideal (i.e., it has neglectable viscosity $\nu = 0$) and that the external force in the Navier-Stokes Eq. (2.4) is gravity $\mathbf{F}_{\text{ext}} = (0, 0, -\rho g) = \nabla(-\rho g z)$, then the Navier-Stokes equation takes the form

$$\frac{\partial}{\partial t}\nabla\Phi + \frac{1}{2}\nabla\left((\nabla\Phi)^2\right) = -\frac{1}{\rho}\nabla p + \frac{1}{\rho}\nabla(-\rho g z). \tag{2.6}$$

By collecting the terms on one side and integrating over the spatial dimensions, the Bernoulli equation is obtained,

$$\frac{\partial}{\partial t}\Phi + \frac{1}{2}(\nabla\Phi)^2 + \frac{1}{\rho}p + gz = \text{const.} \tag{2.7}$$

A priori, the constant on the right hand side may be time-dependent $C = C(t)$, but this time dependency may be embedded in a field redefinition $\Phi' = \Phi - \int_{t_0}^{t} C(\tau)d\tau$. When multiplied with the density, the second term can be seen to represent the kinetic energy $\rho\mathbf{u}^2/2$; whereas the term $\rho g z$ represents the potential energy. As we will come back to in Section 2.1.2, when computing hydrodynamic forces, the Bernoulli equation can be used to compute the pressure in the fluid domain.

At the free surface, the pressure equals the atmospheric pressure, $p = p_{\text{atm}}$. To find the constant C on the right hand side of the Bernoulli equation, consider the static case where there are no waves, i.e., there is no fluid velocity $\mathbf{u} = 0$, ϕ is constant and $z = 0$ at the free surface, see Figure 2.2. This implies that $C = \frac{1}{\rho}p_{\text{atm}}$, which further implies that generally, at the free surface $z = \eta(x, y, t)$, the dynamic boundary constraint holds,

$$\frac{\partial}{\partial t}\Phi + \frac{1}{2}(\nabla\Phi)^2 + g\eta = 0 \quad \text{at } z = \eta(x, y, t). \tag{2.8}$$

At any fixed, rigid boundary in the fluid domain, such as the sea bed, the fluid is constrained such that it cannot penetrate the boundary. In other words, the fluid velocity in the direction of the rigid boundary must vanish,

$$\frac{\partial\Phi}{\partial\mathbf{n}} = 0, \tag{2.9}$$

where **n** is the normal of the boundary pointing in towards the fluid domain. Note that in many applications in CFD, the non-penetration constraint (2.9) is replaced by a more conservative no-slip condition, where the relative fluid velocity is zero in all directions at rigid walls. In addition, the fluid particles should stay in the water, i.e., the kinematic constraint is imposed such that the vertical velocity of a fluid particle at the free surface, $u_z = \partial\Phi/\partial z$ should equal the vertical velocity of the surface itself, $\dot{\eta}(t)$,

$$\frac{\partial\Phi}{\partial z} = \frac{\partial\eta}{\partial x}\frac{\partial\Phi}{\partial x} + \frac{\partial\eta}{\partial y}\frac{\partial\Phi}{\partial y} + \frac{\partial\eta}{\partial t} \quad \text{at } z = \eta(x,y,t), \tag{2.10}$$

where it was also used that the fluid velocity components can be written in terms of the velocity potential, $\dot{x}(t) = u_x = \partial\Phi/\partial x$.

In total, the fluid is governed by the Laplace Eq. (2.5) together with the boundary constraints (2.8) and (2.10) at the free surface and (2.9) at any rigid boundary. If the rigid boundary is moving, a more general form of the boundary constraint (2.9) is valid where the velocity of the fluid equals the velocity of the moving boundary.

Linearisation Potential flow theory relies on the assumptions of irrotational, inviscid, and incompressible fluid, but is still described by non-linear partial differential equations. To simplify the non-linear boundary constraints (2.8) and (2.10) at the free surface, a further assumption on non-steep waves is required, i.e., that the wave height H is small in relation to the wave length λ, $H \ll \lambda$. A small parameter

$$\epsilon = ka \ll 1 \tag{2.11}$$

is often defined, where $k = 2\pi/\lambda$ is the wave number and $a = H/2$ the wave amplitude. The fluid potential and the surface elevation can then be expanded as perturbations around the still free surface $z \approx 0$ and the first-order approximation taken. In practice, this amounts to neglecting all non-linear terms in Eqs. (2.8) and (2.10) since they are small. The resulting linear boundary constraints at the free surface are

$$\frac{\partial\Phi}{\partial t} + g\eta = 0 \quad \text{at } z = 0 \tag{2.12}$$

$$\frac{\partial\Phi}{\partial z} - \frac{\partial\eta}{\partial t} = 0 \quad \text{at } z = 0 \tag{2.13}$$

which can be combined into

$$\frac{\partial^2\Phi}{\partial t^2} + g\frac{\partial\Phi}{\partial z} = 0 \quad \text{at } z = 0. \tag{2.14}$$

Together with the fixed rigid body boundary constraint (2.9) and the Laplace Eq. (2.5) in the full domain, they define linear potential flow theory, also known as Airy wave theory.

As defined by Eq. (2.11), the linearisation relies on a perturbation in a small parameter, which only remains small as long as the waves are non-steep. As the waves become steeper, higher-order non-linear terms should be included in the approximation. This is shown in Figure 2.3, which specifies the validity of linear and
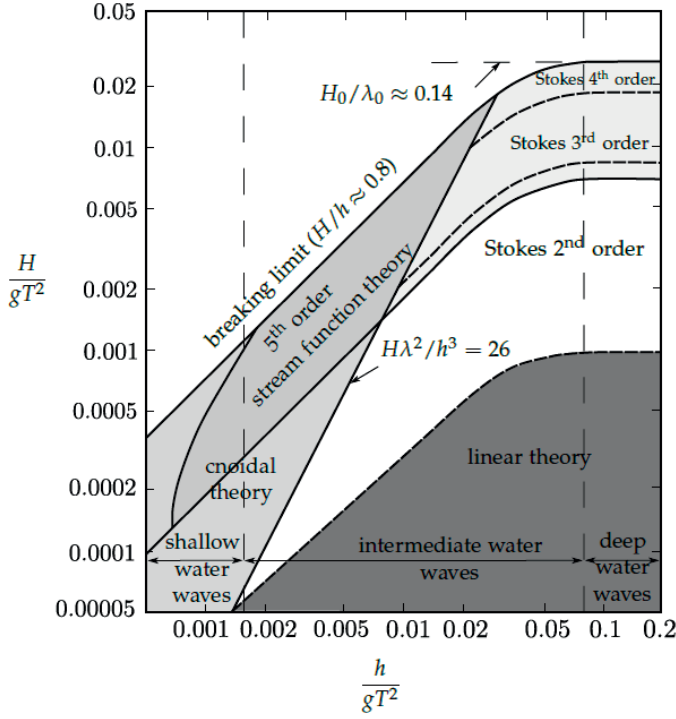
Figure 2.3: Wave model suitability, adapted from [276].

higher-order theories at different water depths and at different wave heights. The validity of different theories describing ocean waves as well as their corresponding solvers will be further discussed in Section 2.5.

2.1.1.3 Dispersive waves

A solution to the Laplace Eq. (2.5) and the linear boundary constraints at the free surface (2.12)–(2.13) and at fixed rigid boundaries (2.9) can be found by separation of variables. Here, the derivation will be considered for a wave propagating only in the x-direction, but the generalisation to wave propagation in both the x and y directions follows analogously.

Consider waves propagating along the x-direction and make the ansatz for a harmonic wave with wave number k and angular frequency ω,

$$\Phi(x,z,t) = Z(z)\sin(kx - \omega t). \tag{2.15}$$

Inserting the ansatz into the Laplace equation gives

$$0 = \nabla^2 \Phi = \left[-k^2 Z(z) + Z''(z) \right] \sin(kx - \omega t), \tag{2.16}$$

implying that the ansatz satisfies the Laplace equation provided that the vertical function $Z(z)$ takes the form $Z(z) = Ae^{kz} + Be^{-kz}$ for some constants A and B. The

boundary constraint at the seabed $z = -h$ further implies that

$$0 = \frac{\partial \Phi}{\partial z}\Big|_{z=-h} = \left[Ake^{-kh} - Bke^{kh} \right] \sin(kx - \omega t) \tag{2.17}$$

which implies that the two constants are related as $A/B = e^{2kh}$. Finally, the potential must satisfy the boundary constraints at the free surface, which in combined forms take the expression

$$0 = \frac{\partial^2 \Phi}{\partial t^2} + g\frac{\partial \Phi}{\partial z}\Big|_{z=0} = \left[-\omega^2 (A+B) + gk(A-B) \right] \sin(kx - \omega t) \tag{2.18}$$

from which follows that

$$\omega^2 = gk\frac{A-B}{A+B} = gk\frac{e^{2kh}-1}{e^{2kh}+1} = gk\tanh(kh). \tag{2.19}$$

With the relationship between the constants A and B inserted, the vertical function takes the form $Z(z) = Be^{kz}(e^{k(z+h)} + e^{-k(z+h)}) = C\cosh(k(z+h))$, where C is some new constant. Often, the constant C is chosen such that $Z(0) = gH/(2\omega)$, which gives the final linear solution: a fluid potential of the form

$$\Phi(x,z,t) = \frac{gH}{2\omega}\frac{\cosh(k(z+h))}{\cosh(kh)}\sin(kx - \omega t) \tag{2.20}$$

satisfies the Laplace Eq. (2.5) and the linear boundary constraints (2.12)–(2.13) at the free surface and the sea bed (2.9), provided that the *dispersion equation* holds,

$$\omega^2 = gk\tanh(kh). \tag{2.21}$$

The dispersion equation relates the frequency of a wave with its wave length, and implies that waves of different wave lengths in general travel with different speeds, i.e., that the phase speed $v_p = \omega/k \propto \lambda$. Waves for which this is true are denoted dispersive. This can be compared with electromagnetic waves in vacuum that are non-dispersive. The dispersion equation for electromagnetic waves in vacuum is $\omega = ck$, where c is the speed of light, implying that the phase speed is always equal to the constant speed of light, $v_p = \omega/k = c$.

The surface elevation corresponding to the fluid potential (2.20) is given by the free surface boundary constraint (2.12),

$$\eta(x,t) = -\frac{1}{g}\frac{\partial \Phi}{\partial t}\Big|_{z=0} = A\cos(kx - \omega t) \tag{2.22}$$

which is a harmonic plane wave with amplitude $A = H/2$, propagating along the x-direction.

The energy available in a harmonic wave is the sum of its kinetic and potential energy. In deep water, it equals

$$E = \frac{1}{8}\rho g H^2 = \rho g \langle \eta^2 \rangle, \tag{2.23}$$

where ρ is the density, H the wave height, and $\langle \eta^2 \rangle$ is the time average of the surface elevation (2.22) squared, also called the variance.

In addition to the energy available in ocean waves per unit ocean area, the transportation of energy, or *energy flux*, is a relevant parameter for wave energy applications. The average energy transported by the per-unit frontage of the incident wave can be calculated as [226, 839]

$$J = \frac{\rho g^2}{4\omega}|A|^2, \tag{2.24}$$

in deep water, where A is the complex wave elevation, and

$$J = \frac{\rho g^2}{4\omega}D(kh)|A|^2, \tag{2.25}$$

in finite-depth water, where $D(kh)$ is the depth function

$$D(kh) = \tanh(kh)\left[1 + \frac{2kh}{\sinh(2kh)}\right]. \tag{2.26}$$

which is a function of the depth h and asymptotic to 1 in deep water. Note that J will be used in Chapters 3, 5, and 8 in the definitions of capture width, interaction factors, etc.

2.1.1.4 Wave spectra and wave parameters

From the linearity of the Laplace equation and the boundary constraint, solutions can be superposed into new solutions. In general, ocean waves consist of sums of many harmonic waves of the form (2.20), travelling in many directions simultaneously. Since ocean waves are dispersive, when they travel over long distances they will separate according to their frequency. When reaching a distant point, the resulting superposition will consist of waves with similar frequencies, the so-called swells, see Figure 2.1.

Consider an irregular ocean surface composed of many harmonic waves (2.22) of amplitudes A_n and angular frequency $\omega_n = nd\omega$. At a certain point (x, y), the time-dependent surface elevation is given by $\eta(t) = \sum_n A_n \cos(\omega_n t + \varphi_n)$, where φ_n are phases. The variance of the surface elevation for the irregular waves is

$$\langle \eta^2 \rangle = \frac{1}{T}\int_0^T \left[\sum_{n=0}^{\infty} A_n \cos(\omega_n t + \varphi_n)\right]\left[\sum_{n=0}^{\infty} A_m \cos(\omega_m t + \varphi_m)\right]dt = \sum_{n=0}^{\infty}\frac{1}{2}A_n^2, \tag{2.27}$$

where the orthonormality of trigonometric functions was used, implying that the only contribution from the product of the cosine functions is when $m = n$. By comparing (2.23) and (2.27), the conclusion can be drawn that the energy of the nth wave component is given in terms of the amplitude of the wave component as $E_n = \frac{1}{2}\rho g A_n^2$.

At this point a new function $S_\eta(f_n)$, called the spectral density function, can be defined as $S_\eta(f_n)df = \frac{1}{2}A_n^2$ with units m^{2}s, so that

$$\langle \eta^2 \rangle = \sum_{n=0}^{\infty}\frac{1}{2}A_n^2 = \frac{1}{\rho g}\sum_{n=0}^{\infty}E_n = \sum_{n=0}^{\infty}S_\eta(f_n)df, \tag{2.28}$$

where $f_n = \omega_n/2\pi$ are the frequencies. The spectral density function is proportional to the energy density for each wave component f_n. When the frequency step becomes infinitesimally small $df \to 0$, the sum can be written as an integral, and the variance, and thus the energy of the irregular waves, can be expressed as

$$E = \rho g \langle \eta^2 \rangle = \rho g \int_0^\infty S_\eta(\omega) d\omega. \tag{2.29}$$

A harmonic wave is characterised by its wave height, wave length, and period (and the latter two parameters are related by the dispersion equation). Clearly, irregular waves cannot be described by a single wave height and period. Instead, these parameters must be defined statistically, which is undertaken in terms of so-called spectral moments. The nth spectral moment is defined in terms of the spectral density function and the wave frequency as

$$m_n = \int_0^\infty f^n S_\eta(f) df. \tag{2.30}$$

From comparison with Eq. (2.29), it is clear that the zeroth spectral moment is proportional to the energy of the irregular waves,

$$m_0 = \int_0^\infty S_\eta(f) df = \langle \eta^2 \rangle = \frac{1}{\rho g} E. \tag{2.31}$$

The significant wave height is defined in terms of the zeroth spectral moment as

$$H_s = 4\sqrt{m_0}, \tag{2.32}$$

sometimes also denoted H_{m0}. Its definition has historical reasons. An older definition of significant wave height is the average wave height of the highest 1/3rd of the waves, denoted $H_{1/3}$. This was the wave height "estimated by a well-trained observer". The new definition in terms of spectral moments agrees with the historical one within a few percent, $H_s \approx H_{1/3}$.

The energy period of irregular waves is defined as

$$T_e = \frac{m_{-1}}{m_0}. \tag{2.33}$$

It is the period with which a single harmonic wave would have the same energy as the irregular waves. Another useful statistical property is the average up- or down-crossing periods. An up-crossing period is the time between when the surface elevation passes from $z < 0$ to $z > 0$, to the next such event. The up-crossing period is defined as the average of those periods, and can be written in terms of spectral moments as $T_z = \sqrt{m_0/m_2}$. The average crest period $T_c = \sqrt{m_2/m_4}$ is defined as the length of the wave record divided by the number of crests within that record, and the peak period $T_p = 1/f_p$ is defined as the period for which the spectral density has a peak, $S'(f_p) = 0$.

From the definition of the significant wave height and Eq. (2.31), the energy in irregular ocean waves beneath a unit area is given by
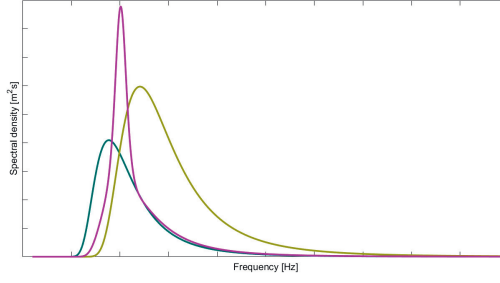
$$E = \frac{1}{16} \rho g H_s^2, \tag{2.34}$$

Figure 2.4: Different wave spectra of the form in Eq. (2.35) for different values of the constants A and B.

which can be compared with the analogous expression for harmonic waves in Eq. (2.23).

As derived above, the irregular ocean waves can be described stochastically in terms of their wave spectra and related wave parameters, such as significant wave height and peak or energy period, and the energy available in ocean waves is directly proportional to the integral of the spectra over all wave frequencies. In general, the different wave components may travel in different directions simultaneously, and the wave spectrum is dependent on direction, $S(\theta, f)$. For a more thorough description of ocean waves and directional wave spectra, the reader is referred to a textbook specific for the subject, such as [587].

From considerations of a finite valued energy and energy flux, and based on empirical studies, it has been found that a typical spectrum can be written in the form

$$S(\omega) = \frac{A}{\omega^5} e^{-B/\omega^4} \qquad (2.35)$$

where A and B are constants that can be determined in different ways, and $\omega = 2\pi f$ is the angular frequency of the wave component. The typical form of such a function can be seen in Figure 2.4. Empirical formulas have been derived from large data sets of realistic wave measurements to find the explicit form of the spectral density functions, and different wave spectra exist that describe waves in different ocean basins to varying degrees of accuracy.

The Bretschneider spectrum was derived in conditions where the wind has only a limited distance to generate the waves [88],

$$S_{\text{Bret}}(\omega) = \frac{5\omega_p^4 H_s^2}{16} \frac{1}{\omega^5} \exp\left(-\frac{5}{4}\left(\frac{\omega_p}{\omega}\right)^4\right) \qquad (2.36)$$

where ω_p is the peak angular frequency. Based on the assumption of a fully developed sea, where equilibrium has been reached between the waves and the wind, the Pierson-Moskowitz spectrum was presented on the form [635]

$$S_{\text{PM}}(\omega) = \frac{\alpha g^2}{\omega^5} \exp\left(-\beta\left(\frac{\omega_0}{\omega}\right)^4\right) \qquad (2.37)$$

where $\alpha = 0.0081$, $\beta = 0.74$, $\omega_0 = g/U_{19.5}$, and $U_{19.5}$ is the wind speed measured at a height of 19.5 m above the sea surface. Another often-used parameter is the wind speed at 10 m above the surface, which in most situations is related to the wind speed at 19.5 m as $U_{19.5} \approx 1.026U_{10}$, where a drag coefficient of $1.3 \cdot 10^{-3}$ was assumed. The peak frequency of the Pierson-Moskowitz spectrum is the one for which $S'(\omega_p) = 0$, which is $\omega_p = 0.844g/U_{19.5}$ rad/s^{-1}.

In the JOint North Sea WAve Project, sharper peaks were observed than were predicted by the Pierson-Moskowitz spectrum, and it was found that the waves were never fully in equilibrium, they continued to develop through non-linear wave interactions, implying also that wave speed can become larger than the wind speed. A modified spectrum with a peak enhancement factor was developed, the so-called JONSWAP spectrum [339],

$$S_{\text{JONSWAP}}(\omega) = \frac{\alpha g^2}{\omega^5} \exp\left(-\beta \left(\frac{\omega_p}{\omega}\right)^4\right) \gamma^r \qquad (2.38)$$

where the parameters were defined as $\alpha = 0.076(U_{10}^2/gF)^{0.22}$, where U_{10} is the wind speed at 10 m height, $\beta = 1.25$, $\gamma = 3.3$, and $r = e^{-(\omega-\omega_p)^2/(2\sigma^2\omega_p^2)}$ where the parameter $\sigma = 0.07$ for $\omega \leq \omega_p$ (angular frequencies smaller than or equal to the peak angular frequency) and $\sigma = 0.09$ for $\omega > \omega_p$.

The *fetch F* is defined as the distance over which the wind blows with constant velocity. As discussed above, the waves of relevance for wave energy are generated by winds, which is reflected in the form of the empirical spectra. The stronger the wind, the longer the duration of the wind, and the longer the distance over the ocean surface the wind has blown (the so-called fetch), the bigger the resulting waves will be.

2.1.2   Wave-structure interaction

Once the wave field is obtained, the wave-structure interaction and the dynamics of a structure due to the hydrodynamic forces can be studied.

2.1.2.1   *Hydrodynamic forces*

Once the equations describing the ocean waves have been solved, the pressure in the fluid can be determined. In the case of the full Navier-Stokes Eq. (2.4), the fluid velocity and the pressure are obtained numerically using a CFD method. In the case of (linear) potential flow theory, solutions to the Laplace Eq. (2.5) and the boundary constraints (2.9), (2.12)–(2.13) can be solved either by analytical or numerical methods, and the pressure can be obtained from the Bernoulli Eq. (2.7).

The force and force moment on a structure in a fluid is given by the fluid pressure integrated along the wetted surface S of the structure as

$$\mathbf{F} = \iint_S p d\mathbf{S} \qquad (2.39)$$

where for the force vector $d\mathbf{S} = \mathbf{n}dS$, $\mathbf{n}$ being the normal vector pointing out from the structure into the fluid, and for the force moment vector $d\mathbf{S} = \mathbf{r} \times \mathbf{n}dS$, where $\mathbf{r}$ is the moment arm pointing from the axis of rotation to the surface element dS.

From this point, the fluid will be restricted to the case of potential flow theory. The total fluid pressure is the sum of the hydrodynamic pressure due to the waves and the hydrostatic pressure. From Eq. (2.7), the hydrodynamic pressure can be obtained as

$$p_{\mathrm{dyn}} = -\rho \left(\frac{\partial \Phi}{\partial t} + \frac{1}{2}(\nabla \Phi)^2 \right). \tag{2.40}$$

As discussed in the previous section, in linear potential flow theory the non-linear term can be neglected and the dynamic pressure can be described in terms of the first term. Furthermore, due to the linearity, the fluid velocity potential can be divided into potentials corresponding to incident, scattered and radiated waves,

$$\Phi = \Phi_I + \Phi_S + \Phi_R. \tag{2.41}$$

The scattered waves appear when waves are scattered off a fixed structure, and the radiated waves are due to the structure's own motion in the water.[1]

The force and force moments of Eq. (2.39) can then be separated into forces resulting from incident and scattered waves off a fixed structure, denoted excitation force $\mathbf{F}_e$, and forces resulting from the motion of the structure in the absence of incident waves, denoted radiation force $\mathbf{F}_r$.

$$\mathbf{F} = \underbrace{-\rho \iint_S \left(\frac{\partial \Phi_I}{\partial t} + \frac{\partial \Phi_S}{\partial t} \right) d\mathbf{S}}_{\mathbf{F}_e} + \underbrace{-\rho \iint_S \frac{\partial \Phi_R}{\partial t} d\mathbf{S}}_{\mathbf{F}_r} \tag{2.42}$$

and analogously for the force moment. In the frequency domain description of the problem, the expressions simplify further, which will be discussed in Section 3.1.2.

The radiation force is usually written as a sum of a term proportional to the acceleration of the structure, added mass, and a term proportional to its velocity, radiation damping. (In the frequency domain, these correspond to the imaginary and real parts of the radiation force, respectively.) The terms *added mass* and *radiation damping* (or radiation resistance) indicate the physical interpretation of the terms: the added mass can be understood as the added inertial force due to the mass of the volume of water following the body's oscillation, whereas the radiation damping can be understood as the damping of the oscillatory motion due to the emitted energy in terms of radiated waves.

2.1.2.2 Hydrostatic forces

The hydrostatic forces are due to the fluid loading acting on a body when placed in still water. It originates from the static-pressure term $-\rho g z$ in Eq. (2.6), because

---

[1]Note that the term *diffracted* waves is sometimes used to describe the sum of incident and scattered waves, $\Phi_D = \Phi_I + \Phi_S$, whereas sometimes the opposite meaning of diffracted and scattered waves is used, i.e., $\Phi_S = \Phi_I + \Phi_D$.

the body's wet surface experiences a varying hydrostatic pressure as a result of its oscillation. The hydrostatic forces can be determined using the same method for the hydrodynamic forces, and can be expressed as

$$\mathbf{F}_s = -\rho g \iint_S z \mathrm{d}\mathbf{S}, \tag{2.43}$$

and analogously for the force moment.

2.1.2.3 Hydrodynamic responses

The motion of a rigid body can be characterised by six components corresponding to six degrees of freedom (DoF) or modes of (oscillatory) motion. For a vessel like an elongated body (directed parallel to the x axis, as indicated in Figure 2.5), the six modes numbered 1 to 6 are named surge, sway, heave, roll, pitch, and yaw, respectively.
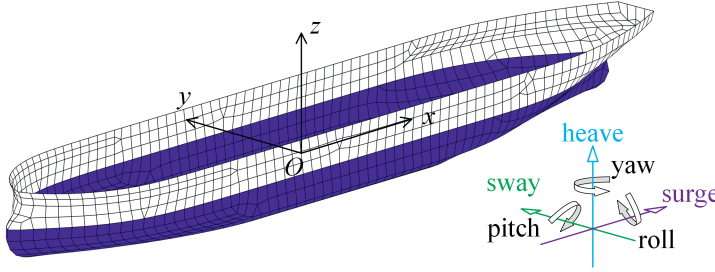

Figure 2.5: A vessel in still water with its wet surface marked in blue colour. A rigid body has six modes of motion: surge, sway, heave, roll, pitch, and yaw.

A six-dimensional generalised velocity vector $\dot{\mathbf{x}}$ is introduced with components

$$(u_1, u_2, u_3) = (U_x, U_y, U_z) = \bar{U}, \tag{2.44}$$

$$(u_4, u_5, u_6) = (\Omega_x, \Omega_y, \Omega_z) = \bar{\Omega}, \tag{2.45}$$

where $\bar{U}$ is the velocity of a reference point and $\bar{\Omega}$ is the angular velocity vector corresponding to rotation about the reference point. Note that the components numbered 1 to 3 have SI units of m/s; whereas the remaining components numbered 4 to 6 have SI units of rad/s.

From Newton's second law, the dynamic equation for an oscillating body may be written as

$$\mathbf{M}\ddot{\mathbf{x}} = \mathbf{F}_e + \mathbf{F}_r + \mathbf{F}_s + \mathbf{F}_p + \mathbf{F}_c + \mathbf{F}_m + \mathbf{F}_v, \tag{2.46}$$

where $\mathbf{M}$ denotes the inertia of the oscillating body. $\mathbf{F}_e$ and $\mathbf{F}_r$ represent the six-dimensional generalised vectors of the wave excitation forces/moments and wave radiation forces/moments, respectively (see Eq. (2.42)). $\mathbf{F}_s$ denotes the hydrostatic buoyancy force vector (see Eq.(2.43)).

Apart from the fluid force, including both the total wave force, $\mathbf{F}_e + \mathbf{F}_r$, and the hydrostatic buoyancy force, $\mathbf{F}_s$, some additional forces are considered as the four

last terms in Eq. (2.46). $\mathbf{F}_p$ denotes a load force due to some purpose. It could be a power take-off (PTO) system necessary for the conversion of wave energy and/or a control force intended, for example, to reduce the oscillation of a floating body or to enhance wave power absorption of the wave energy device. A load force induced by interconnected constraint may also be considered as a component of this kind of force; where $\mathbf{F}_m$ represents the mooring force and $\mathbf{F}_v$ represents an unavoidable viscous effect.

2.2 LINEAR POTENTIAL FLOW THEORY SOLVERS

For many wave energy applications, ocean waves can, to a good approximation, be described by linear potential flow theory, as was discussed in Section 2.1.1.2, where the equations governing linear potential flow theory were derived. One solution representing a harmonic wave was derived in Section 2.1.1.3 to illustrate the dispersion equation. Here, more general solutions to the theory will be derived, using analytical methods in Section 2.2.1 and the numerical boundary element method in Section 2.2.2.

2.2.1 Analytical solutions

To solve the equations of motion (2.46), the dynamical forces must be determined. From Eq. (2.42), the forces can be obtained as integrals of the fluid velocity potentials. The fluid potentials should satisfy the Laplace Eq. (2.5) and the boundary constraints at fluid boundaries, including the free surface. Again, the problem will be restricted to the linear potential flow theory, where the boundary constraints at the free surface take the form (2.14).

A common strategy is to solve the potentials in the frequency domain using separation of variables. Using Fourier transform, the fluid potential can be considered in the frequency domain,

$$\phi(\mathbf{x}) = \int_{-\infty}^{\infty} \Phi(\mathbf{x}, t) e^{\mathrm{i}\omega t} dt, \tag{2.47}$$

where the frequency dependence in $\phi(\mathbf{x})$ is implicit. In the frequency domain, the time derivative translates to multiplication with the frequency,

$$\frac{\partial}{\partial t} \Phi(\mathbf{x}, t) = \int_{-\infty}^{\infty} [-\mathrm{i}\omega \phi(\mathbf{x})] e^{-\mathrm{i}\omega t} dt, \quad \frac{\partial}{\partial t} \leftrightarrow -\mathrm{i}\omega. \tag{2.48}$$

To find a potential satisfying both the Laplace equation and the linear boundary constraints, an ansatz can be made in the form

$$\phi(x, y, z) = W(x, y) Z(z). \tag{2.49}$$

Inserted back into the Laplace equation and separating the horizontal and vertical coordinates reveals that

$$\frac{1}{W} \left(\frac{\partial^2 W}{\partial x^2} + \frac{\partial^2 W}{\partial y^2} \right) = -\frac{1}{Z} \frac{\partial^2 Z}{\partial z^2} = \alpha \tag{2.50}$$

where α is a constant. Thus, the vertical eigenfunctions satisfy the differential equation $Z''(z) + \alpha Z(z) = 0$ and take the form of trigonometric functions,

$$Z(z) = C \cos(\alpha z + \beta). \tag{2.51}$$

When inserting this expression into the boundary constraint at the sea bed (2.9),

$$0 = \frac{\partial \phi}{\partial z}\bigg|_{z=-h} = -W(x,y)C\sin(-\alpha h + \beta), \tag{2.52}$$

which is satisfied if $\beta = \alpha h$. Furthermore, the linear boundary constraint at the free surface (2.14) in the frequency domain takes the form

$$0 = -\omega^2\phi + g\frac{\partial \phi}{\partial z}\bigg|_{z=0} = -[\omega^2 + g\alpha\tan(\alpha h)]W(x,y)Z(z) \tag{2.53}$$

which is satisfied if $\omega^2 = -g\alpha\tan(\alpha h)$. To find which values of the constant α satisfy this relationship, the case when α is a real, positive number is considered. In that case, for each value of the angular frequency ω, there are infinitely many solutions $\alpha = k_m > 0$ to the equation

$$\omega^2 = -gk_m\tan(k_m h) \tag{2.54}$$

where each solution lies within the range $k_m \in \left(\frac{\pi}{h}\left(m - \frac{1}{2}\right), \frac{m\pi}{h}\right)$. Negative and real values of α correspond to the same solutions. In the case when α is a complex valued number, we write $\alpha = -\mathrm{i}k$, giving the expression

$$\omega^2 = gk\tanh(kh) \tag{2.55}$$

which was also derived in Eq. (2.21). Eqs. (2.54) and (2.55) are called the dispersion equation. For each value of the angular frequency ω, there is a unique solution $k > 0$ satisfying the dispersion Eq. (2.55). The two cases of real and complex solutions can be combined into one, $Z(z) = C_m\cos(k_m(z+h))$, with $k_0 = -\mathrm{i}k$. Typically, the constants C_m are chosen such that the vertical eigenfunctions are orthogonal,

$$Z_m(z) = \frac{\cos(k_m(z+h))}{\cos(k_m h)}, \qquad m \geq 0, \quad k_0 = -\mathrm{i}k. \tag{2.56}$$

Note that in the case of $m = 0$ (i.e., the complex root of the dispersion solution), the vertical function takes the form of a hyperbolic cosine, $Z_0(z) \propto \cosh(k(z+h))$, also shown in Eq. (2.20).

The general solution to the horizontal part $W(x,y)$ of the fluid potential will take different forms depending on the geometry of the problem. In Section 2.1.1.3, it could be seen that if the function were independent of y, a solution could be found in a simple form of a trigonometric function, representing a plane wave propagating along the x-direction.

Many fluid systems relevant for wave energy can be described using cylindrical geometry; for instance, waves scattered off pillars with circular cross sections, or waves

radiated from a stone dropped in a pond or from an oscillating cylindrical buoy. In such cases, it is appropriate to seek the horizontal function in cylindrical coordinates, as a product between a radial and an angular function, $W(x,y) = R(r)\Theta(\theta)$. When inserted into the Laplace Eq. (2.50) in cylindrical coordinates and separating the radial and angular parts, the following equations are obtained,

$$\frac{r^2}{R(r)}\left[R''(r) + \frac{1}{r}R'(r) - k_n^2 R(r)\right] = -\frac{1}{\Theta(\theta)}\Theta''(\theta) = n^2 \tag{2.57}$$

where n is a constant and k_n are the solutions to the dispersion Eqs. (2.54)–(2.55) obtained earlier. For the angular function, this is satisfied by a function of the form

$$\Theta(\theta) = Ce^{in\theta}, \tag{2.58}$$

where C is a constant and n an integer to satisfy the periodicity condition $\Theta(\theta+2\pi) = \Theta(\theta)$. The radial function represents a modified Bessel equation, which is solved by modified Bessel functions,

$$R(r) = AK_n(k_m r) + BI_n(k_m r). \tag{2.59}$$

For the fundamental solution $k_0 = -ik$ of the dispersion equation, the modified Bessel functions correspond to a Hankel function of the first kind, $K_n(k_0 r) \propto H_n^{(1)}(kr)$, and a Bessel function of the first kind, $I_n(k_0 r) \propto J_n(kr)$, respectively.

To summarise, the fluid velocity potential that satisfies the Laplace equation and the linear boundary constraints in a cylindrical coordinate system takes the form

$$\phi(r,\theta,z) = \sum_{m=-\infty}^{\infty}\sum_{n=-\infty}^{\infty}[A_{mn}K_n(k_m r) + B_{mn}I_n(k_m r)]e^{in\theta}Z(z), \tag{2.60}$$

where the vertical eigenfunction takes the expression in (2.56). The case $k_0 = -ik$ corresponds with the dispersion Eq. (2.55) to propagating modes represented by Hankel functions and Bessel functions of the first kind, whereas the higher modes $k_m > 0$ correspond to the dispersion Eq. (2.54) with $m > 0$ and evanescent modes represented by modified Bessel functions.

In presence of one or several bodies, body boundary constraints and requirement of continuity of the velocity potentials over fluid domains can be used to determine the unknown coefficients A_{mn} and B_{mn} in Eq. (2.60). In some cases, such as a bottom-mounted cylinder, this can be done exactly, whereas in the case of a floating truncated cylinder the solution can be found semi-analytically by truncating the infinite sums in Eq. (2.60) and solving the resulting system of linear equations.

For more in-depth information and for solutions in other geometries and coordinate systems, the reader is referred to the excellent textbook [450]. The analytical solution will be extended to arrays of floating structures in Chapter 8.

2.2.2 Boundary element method

In addition to the analytical techniques, e.g., the method of separation of variables, a more general way is to apply a standard boundary element method (BEM). Without

being limited to regular geometries, BEM has the advantage that all the unknowns are restricted on specified boundaries so that the preprocessing work such as meshing can be extremely straightforward. In BEM, the boundary integral equations are derived via Green's theorem within a confined or unconfined space. The boundary integral equations can be numerically solved by discretising the boundaries into a number of geometrical and physical elements. These elements can be approximated using Lagrange interpolating polynomials, B-splines, etc., depending on the requisite accuracy.

2.2.2.1 Boundary integral equation

The complete linear frequency-domain problem is comprised by the Laplace Eq. (2.5), the free-surface boundary conditions (2.12) and (2.13), the rigid body boundary condition (2.9), plus an appropriate wave radiation condition such as the Sommerfeld condition (2.61) in the far-field,

$$\lim_{R \to \infty} \left[\sqrt{kR} \left(\frac{\partial \phi}{\partial R} - ik\phi \right) \right] = 0, \tag{2.61}$$

where R refers to the distance away from the body. Based on Green's second theorem, the radiated and diffracted wave velocity potentials on the immersed body surface S_B can be solved by a set of boundary integral equations. The integral equations can be with respect to either a distribution of sources

$$2\pi\sigma(\boldsymbol{x}) + \iint_{S_B} \sigma(\boldsymbol{\xi}) \frac{\partial G(\boldsymbol{\xi};\boldsymbol{x})}{\partial n_{\boldsymbol{x}}} dS_{\boldsymbol{\xi}} = V_n, \tag{2.62}$$

or mixed sources and dipoles

$$2\pi\phi(\boldsymbol{x}) + \iint_{S_B} \phi(\boldsymbol{\xi}) \frac{\partial G(\boldsymbol{\xi};\boldsymbol{x})}{\partial n_{\boldsymbol{\xi}}} dS_{\boldsymbol{\xi}} = \iint_{S_B} V_n(\boldsymbol{\xi}) G(\boldsymbol{\xi};\boldsymbol{x}) dS_{\boldsymbol{\xi}}, \tag{2.63}$$

where $\boldsymbol{\xi}$ refers to the source point on the body surface and $\boldsymbol{x}$ the field point in the fluid domain or on the body surface, and V_n denotes the respective normal velocity on the body surface. It has been proved that the mixed source-dipole distribution method is more accurate than the source distribution method [154]. Eq. (2.12) can be discretised using splines or polynomials. Taking the most popular constant panel method for example (i.e., the zeroth-order Lagrange interpolating polynomials), the discrete form of Eq. (2.12) is

$$2\pi\phi(\boldsymbol{x}_i) + \sum_{j=1}^{N} D_{ij}\phi(\boldsymbol{x}_j) = \sum_{j=1}^{N} S_{ij} V_n(\boldsymbol{x}_j), (i = 1, 2, ..., N), \tag{2.64}$$

where N is the number of panels on the immersed body surface. The integration of sources and dipoles over each panel can be represented by

$$S_{ij} = \iint_{S_{B,j}} G(\boldsymbol{\xi};\boldsymbol{x}_i) dS_{\boldsymbol{\xi}}, \tag{2.65}$$

$$D_{ij} = \iint_{S_{\mathrm{B},j}} \frac{\partial G(\boldsymbol{\xi};\boldsymbol{x}_i)}{\partial n_\xi} \mathrm{d}S_{\boldsymbol{\xi}}, \tag{2.66}$$

where $S_{\mathrm{B},j}$ denotes the jth panel surface.

2.2.2.2 Removal of irregular frequencies

Directly solving of Eq. (2.63) leads to substantial errors in the neighbourhood of the so-called "irregular frequencies". This phenomenon is caused by the waterplane section of the members of floating bodies that intersects the free water surface. The irregular frequencies actually coincide with the eigenfrequencies of the corresponding sloshing modes of the interior tank (assuming flow filling inside the tank).

There are several approaches to prevent these numerical errors. Ref. [881] presents the modified Green function method and the extended integral equation method (the latter has later been applied in WAMIT). Ref. [446] gives a comprehensive comparison between the extended integral equation method and the overdetermined integral equation method, and concludes that the overdetermined integral equation method is more computationally efficient, as it only requires a few discrete points on the waterplane area, in contrast with hundreds and thousands of waterplane panels in the extended integration method.

The overdetermined integral equation method assumes that the potentials on the interior water plane are zero. By applying Green's theorem in the interior domain of the floating body, an additional boundary integral equation is introduced in a combined application with Eq. (2.63):

$$\iint_{S_{\mathrm{B}}} \phi(\boldsymbol{x}) \frac{\partial G(\boldsymbol{\xi};\boldsymbol{x})}{\partial n_{\boldsymbol{\xi}}} \mathrm{d}S_{\boldsymbol{\xi}} = \iint_{S_{\mathrm{B}}} V_{\mathrm{n}},(\boldsymbol{\xi}) G(\boldsymbol{\xi};\boldsymbol{x}) \mathrm{d}S_{\boldsymbol{\xi}}, (\boldsymbol{x} \in S_{\mathrm{WP}}, \boldsymbol{\xi} \in S_{\mathrm{B}}), \tag{2.67}$$

where S_{WP} denotes the interior waterplane area. By choosing several discrete points (say, M points) on S_{WP}, a set of over-determined linear algebraic equations can be constructed, which finally leads to the following linear algebraic system:

$$\sum_{n=1}^{N} \left\{ \sum_{m=1}^{M+N} A_{mn} A_{mp} \right\} \phi_k(\boldsymbol{x}_n) = \sum_{m=1}^{M+N} A_{mp} B_k(\boldsymbol{x}_m), (p = 1, 2, ..., N), \tag{2.68}$$

Eq. (2.68) can regularly be solved without any problem. In addition to the advantage of less computational cost, the overdetermined integration method avoids evaluation of the logarithmic singularity of free-surface Green's function occurring in the limiting case when the panel is on the free surface. Interested readers can refer to Refs. [429, 454, 446] for the implementation details of this method.

2.2.2.3 Calculating free-surface Green's functions

The computational burden of BEM mainly lies in two aspects, namely the computation of free-surface Green's functions and solution of the resultant linear algebraic system. This holds true for both frequency-domain and time-domain BEMs. The infinite interval of the integral, the oscillating nature, and the singularity behaviour of

the integrand are the three key difficulty points in calculating free-surface Green's functions.

There have been numerous works on developing efficient and accurate algorithms for free-surface Green's functions, for the deepwater condition (e.g., [572, 843]), and for the finite-depth water condition ([572, 120, 458, 473]). In general, the calculation strategies can be categorised into several types (in particular for finite-depth Green's function): (1) extracting slow-varying components from the Green function and using a Chebyshev or multi-dimensional polynomial method to approximate them (e.g., [572, 120, 473]); (2) applying asymptotic or power series expansions, such as eigenfunction expansions, rapid convergent series, or a combination with other numerical acceleration algorithms in different subregions (e.g., [634, 448, 456]); (3) decomposing the principal-value integral into two parts by subtracting a special term from the integrand and applying a direct Gauss-Laguerre quadrature to the numerical integration (e.g., [200, 455]). In order to reduce the repeated effort in implementation of these algorithms, [761] and [447] released their open-source codes for the deepwater Green function, and [458] released an open-source code for the finite-depth Green function.

2.2.2.4 *Resolving linear algebraic system*

As we may know, a direct solver such as Gauss elimination is generally robust but requires $O(N^3)$ computations (N denotes the matrix size), while some iterative methods can reduce the effort to $O(N^2)$ operations. The linear algebraic system, constituted by Eq. (2.63) for a submerged body or Eq. (2.63) and Eq. (2.68) for a floating body, is a full-rank dense complex system. For a large-scale computation of three-dimensional offshore structures, a direct inversion or inefficient iteration of such a large, dense system of linear equations with $O(N^4)$ unknowns for a set of wave frequencies is seemingly prohibitively time consuming even with modern computers. Note that no matter which method to remove irregular frequencies is employed, the condition number of the resultant linear algebraic system always increases. This means that an iterative method, such as the GMRES method, is no longer appropriate to solve equations like Eq. (2.68), because of the ill conditions. In addition, considering the usual cases when the radiation-diffraction problem needs to be solved with multiple wave headings for each single wave frequency, the computation effort of using either a direct method or an iterative method is still not acceptable because it needs to solve the linear equations for every wave heading in succession.

Considering all the reasons above, several improved options are recommended to solve the problem. The first one is to apply an LU decomposition (e.g., the "ZGETRF" subroutine of LAPACK) for the left-hand side matrix, since it needs to decompose the matrix only once for each wave frequency. This decomposition can be applied to calculate the wave forces for a distribution of wave headings via a forward and backward substitution (e.g., the "ZGETRS" subroutine of LAPACK) for triangular matrices (L and U), which can be solved directly without using the Gaussian elimination process. The second option is to use a preconditioned iterative method. However, one needs to be especially careful in choosing an appropriate preconditioner.

2.2.2.5 *Parallelisation on multi-core machines*

The problems to be solved are often of a very large size such that resolving the resultant linear systems requires huge computational resources. Nowadays, with the facility of a fast multi-core computer, it is natural to maximise the advantages of the current hardware technology in our computations. A large portion of the programs that people write and run daily are serial programs, especially in the marine hydrodynamic field to the best of the author's knowledge. Applying a parallelisation technique enables a better performance of the numerical code on multiple processors. Taking into consideration that in a typical case, the number of panels involved in the hydrodynamic computation is usually below ten thousand to thirty thousand and that off-the-shelf computation machines contain multiple processors, the open multi-processing (OpenMP) technique is considered to be an appropriate option for the BEM solver in marine hydrodynamics. Furthermore, in the case of a large-scale computation on a cluster of machines, the message passing interface (MPI) standard is recommended for use in programming. However, OpenMP needs much less effort than MPI as the latter can request substantial modifications on the code architecture.

2.2.2.6 *Useful references and tools*

Inspired by Hess and Smith (1964) [351], many numerical solvers based on BEM arose from the mid 1980s. In general, these solvers can be categorised as commercial, in-house, and open-source. In Table 2.1, a comparison is given regarding the mainstream BEM solvers that are available to users in the ocean engineering and renewable energy community. Note that in-house codes (DIFFRACT [188], WAFDUT [763], etc.) are not listed here as they cannot be publicly accessed. Moreover, some derived versions of these codes are neither included, such as WADAM [180] (a descendant of WAMIT [431]), OpenWARP [492] and Capytaine [16] (descendants of NEMOH [46]) since the main functionalities are basically the same as their parents'.

In addition, there are also some other resources that the users can find to assist their hydrodynamic analysis via BEM, such as mesh processing (BEMRosseta, BEMIO, Gmsh), post-processing (BEMRosseta), etc.

2.3 COMPUTATIONAL FLUID DYNAMICS

2.3.1 Governing equations

The Navier-Stokes and the continuity equations, expressed in Eq. (2.4) and (2.1) for incompressible flow, are the fundamental equations used in computational fluid dynamics (CFD) to generate a model of the viscous fluid flow.

In addition, an energy equation can be derived using the principle that energy must be conserved within a closed system, implying that further flow dependency characteristics such as compressibility or thermal effects can also be modelled using this system of equations.

Together with the energy equation, Eqs. (2.1) and (2.4) form a system of coupled partial differential equations that can be used to describe the motion of a viscous flow. Nevertheless, no general closed-form solution to this system of partial differential

Table 2.1: Comparison of the public-available mainstream BEM solvers in the frequency-domain.

Properties	WAMIT	AQWA	Hydrostar	Nemoh	HAMS
Approach	Potential and source formulation	Source formulation	Source formulation	Source formulation	Potential formulation
Discretisation	Constant panel or B-splines	Constant panel	Constant panel	Constant panel	Constant panel
Nonlinearity	Full QTF	Mean drift	Full QTF	Mean drift	Linear
Forward speed	Encounter frequency	Encounter frequency	Encounter frequency	No	No
Radiation-diffraction	Yes	Yes	Yes	Yes	Yes
Removal of irregular frequencies	Yes	Yes	Yes	No	Yes
Body symmetry	Yes	Yes	Yes	Yes	Yes
RAO calculation	Yes	Yes	Yes	Yes	Yes
Free-surface elevation	Yes	Yes	Yes	Yes	Yes
Multi-body modelling	Yes	Yes	Yes	Yes	No
Parallelisation	OpenMP	No	MPI	No	OpenMP
Operating System	Windows/Linux	Windows	Windows	Windows/Linux	Windows/Linux
Access	Commercial	Commercial	Commercial	Open-source	Open-source

equations has been formally proved: in fact it is considered one of the outstanding challenges in mathematics. In Sections 2.1 and 2.2, analytical and numerical solutions to a simplified version of the Navier-Stokes equations were presented, based on approximations of inviscous and irrotational flow. Another approach, which will be discussed in this section, is to consider the full Navier-Stokes equations, solving them by numerical methods. In this approach, the equations are discretised on a grid that represents the fluid domain under consideration and a set of initial conditions, and boundary conditions are stipulated at the domain edges. In this way, a predictive model of the flow is generated.

2.3.2   Volume of fluid method for free-surface flows

As the majority of WECs are surface-piercing devices that convert the free surface kinetic energy to electrical energy, the method by which the free surface is modelled is of paramount importance. The most common technique that is used to compute the free surface motion is the volume of fluid (VOF) method. The method is a numerical technique used to model complex free-surface flows. It is a particularly suitable approach for those simulations in which the free surface boundary undergoes large deformations. In CFD analyses, the transformation of the flow and the subsequent evolution of the free surface is achieved by using a discretisation method to solve a transport equation for the fluid in each cell [292, 356, 511]. The VOF method was primarily developed to overcome the inherent low-resolution problem that occurs at a free surface boundary interface in a multi-phase flow analysis, which arises due to convective flux averaging of flow properties across cell boundaries. This may occur when pure Eulerian or arbitrary Lagrangian-Eulerian (ALE) techniques are employed.

In the volume of fluid method, a function $F(x, y, t)$ is introduced at each grid cell in the domain. The value of this function is defined as unity at any cell entirely occupied by the fluid and zero at any cell completely devoid of fluid. Thus, cells with an intermediate value $0 < F < 1$ are those cells crossed by the free surface boundary. Hence, a cell that has at least one empty neighbour cell ($F = 0$) is by definition a free surface cell. This method allows for the determination of the fluid proportion in each cell through the storage of only a single variable. Because the VOF method only requires the value of the F function to determine the fluid spatial representation, the computational storage requirements are minimised.

Although those cells that contain the free surface are determined from the F function, the orientation of the surface requires additional computation. By calculating the derivatives of the F function at each cell boundary, the free surface normal can be established [684]. The normal direction to the free surface is then the direction in which the F function varies most rapidly (i.e., ∇F). From the value of the F function and the direction of the normal to the boundary, a line cutting the cell can be drawn which represents the free surface boundary. The temporal evolution of the F function and thus the advection of the flow in two dimensional space is governed by the following transport equation:

$$\frac{\partial F}{\partial t} + u\frac{\partial F}{\partial x} + v\frac{\partial F}{\partial y} = 0, \tag{2.69}$$

where u and v are the velocities in the component x and y directions, respectively. Then, as the simulation proceeds in time, the value of function F moves with the fluid. The fluxes across each cell in the fluid domain are then obtained from Eq. (2.69). The value of F is recorded and the simulation is advanced in time by the amount ∂t, at which stage the value of $F(x,y,t)$ is re-computed. OpenFOAM is one of the most commonly used CFD codes for the analysis of wave energy converters. The code employs the VOF method to compute the free surface evolution. In the OpenFOAM InterFOAM solver, the advection of the free surface is controlled by the explicit multidimensional universal limiter with an explicit solution (MULES) algorithm, which is a variation of the flux corrected transport (FCT) scheme [176]. The MULES algorithm relies in a straightforward upwind scheme to the computed advection in the interfacial cells [172]. This scheme ensures the fluxes into or out of a cell are limited to maintain the boundedness of the VOF method, thus ensuring the stability of the numerical code.

The main benefit of the VOF method is that it allows for the analysis of multiple fluid flow interactions (multi-phase flow) within a single simulation. However, it is not a trivial process to incorporate these interactions. A frequently observed problem is the smearing of the fluid boundary. This occurs as a result of diffusion of the transport equation over the mesh cell in which the boundary is located. One method by which this problem can be addressed is by specifying a localised high-resolution mesh in the region where the fluid interface will occur. However, prior knowledge of the evolution of the interfacial region is required for this technique.

Multiphase CFD models can be implemented using either an homogeneous or an inhomogeneous approach. According to the Ansys CFX guide [22], for a given transport process, the homogeneous model assumes that the transported quantities (with the exception of the volume fraction or F function value) for that process are the same for all phases. Thus, a common flow field for velocities, temperature, pressures, etc. is applied to all fluids within the domain. This simplifies the underlying code, which defines the interaction of the fluids at the boundary as a single mass conservation, and a momentum conservation equation is applied to both fluids as opposed to individual conservation equations being applied to each fluid in an inhomogeneous model approach at the fluid interface. The conservation of mass and momentum equations is formulated by summing the averaged fluid properties according to their constituent proportion in the boundary cell. For a two-phase flow, density ρ in the boundary cells is given by:

$$\rho = \sum_{a=1}^{2} r_a \rho_a \tag{2.70}$$

where r_a is the volumetric fraction of each constituent fluid in the free surface boundary cell. The conservation of mass equation for an incompressible fluid in tensor notation is:

$$\frac{\partial(p)}{\partial t} + \frac{\partial(\rho u_i)}{\partial x_i} = 0 \tag{2.71}$$

and the conservation of momentum for an incompressible fluid is:

$$\frac{\partial(\rho u_i)}{\partial t} + \frac{\partial(\rho u_i u_j)}{\partial x_j} = -\frac{\partial p}{\partial x_i} + \frac{\partial \tau_{i,j}}{\partial x_j} + f_i \tag{2.72}$$

where ρ is given in Eq. (2.70) In the domain cells where $F = 1$ or $F = 0$, these equations reduce to the mass and momentum conservation equations for a single-phase fluid. The homogeneous model approach is incorporated into the OpenFOAM multiphase solvers. This limits the relative motion between individual fluids at the boundary interface cells to zero. This is analogous to a "no-slip" boundary condition between the individual fluids at the cells in which the fluid interface is located.

2.3.3   Computational fluid dynamics software

There is a wide variety of CFD software programs used to model wave interactions with energy harvesting devices. Generally, these programs can be classified as proprietary or open-source codes. The most common proprietary packages include Ansys Fluent, Ansys CFX, STAR-CCM+, and FLOW-3D. OpenFOAM is the most common open-source code, with some additional "in-house" codes being developed for specific modelling scenarios. The choice of which software package to employ depends on a number of factors. The first consideration is whether the user has access to the commercial software. The license fees associated with these commercial packages can often incur significant expenses. Another disadvantage of the commercial packages is the difficulties in modifying the underlying code. Frequently, the user has no access to the source code and thus any modifications to the program are prohibited. However, these commercially licenced packages are often more user-friendly, for example with simple-to-use graphical user interfaces (GUIs). In contrast with the commercial codes, the open-source codes do not require expensive licence fees and the source code is readily editable. These points are major advantages of open-source codes. However, many open-source codes do not have a dedicated GUI and many of the commands must be run from the command prompt window or from the terminal window depending on which operating system the software is installed upon. The lack of a GUI is often a disconcerting experience for new users who have little knowledge of CFD programming and who view the experience with trepidation. Nonetheless, it should be remembered that even whilst conducting CFD research on commercial software with a guiding GUI, the researcher should have a deep theoretical knowledge of the mathematics and fundamental physics underlying the simulation scenarios they recreate. The most popular software for the investigation of wave energy converters is the OpenFOAM program. This C++ based code was utilised in approximately 40% of all the published papers on wave energy employing a CFD modelling approach in 2018, and since that time the use of this software code has become even more prevalent. In the following sections, the steps required to create a numerical wave tank and generate a CFD simulation for the analysis of wave energy converters are presented and briefly described. The open-source code OpenFOAM is used for this case study; however, the process is similar for other software programs.

2.3.4 Creating a computational fluid dynamics simulation

The first step in creating a CFD model for the hydrodynamic analysis of a WEC is to generate the numerical wave tank that defines the limits of the numerical model domain. Following on, the domain is discretised by a suitably designed mesh that is capable of capturing the flow physics accurately, in a high-fidelity manner. Suitable initial conditions and boundary conditions are established. The correct numerical schemes should be specified for the solution of governing equations and the mathematical methods and algorithms by which these solutions are computed must be defined.

2.3.4.1 *Numerical wave tank definition*

The numerical wave tank is a computational representation of a physical region, either in the natural environment or in a controlled experimental setting where free-surface gravity waves are manifest. The wave tank may take the form of a flume, whereby one of the tank dimensions (length) is significantly longer than the other two dimensions (width and depth) or a wave basin in which two of the dimensions (length and width) are significantly longer than the third dimension (depth). The tank has a wave generator at one end and may have a wave absorption region at the other end to damp the incident wave energy. Usually, the free surface is open to the atmosphere. The tank should be wide enough that the sidewalls do not influence the study. The characteristics and requirements described in the preceding sentences relate to a physical wave tank; however, the numerical wave tank must also satisfy this criterion. Once the extents of the numerical wave tank are established, the next step is to discretise the domain with a mesh.

2.3.4.2 *Mesh generation*

The software user should first decide if they will utilise the program's built-in mesh generation functionality or if it is more advantageous to use a dedicated meshing software and import the generated mesh into the CFD program. This may depend on the complexity of the mesh and whether the WEC (that is immersed in the wave tank domain) has a highly convoluted geometry that may not be accurately rendered by the built-in meshing utility in the CFD program. Another consideration that influences the meshing process is whether the mesh will be static or dynamic. In most cases, WECs rely on the motion of some floating or submerged device to generate electricity. Therefore, to model the motion of these devices, the mesh must displace or distort in an appropriate manner to capture the device's motion. This requirement of a deformable mesh is not applicable to bottom-mounted or fixed OWCs.

Meshing software   The majority of CFD software, whether commercial or open-source, incorporates a domain meshing functionality. However, as outlined in the previous section, there are situations in which the numerical modeller may choose to use a dedicated mesh generating software. There are a number of mesh

generating and mesh editing programs for this purpose, for example, Pointwise, CF-Mesh+, SALOME etc. OpenFOAM, one of the most commonly used CFD softwares, has a dedicated mesh generator module named *SnappyHexMesh* which is capable of creating a domain mesh fitted to highly complex geometries.

SnappyHexMesh in OpenFOAM   In order to ensure high fidelity results from a numerical simulation, the solid body WEC device that is used for the energy extraction must be represented accurately in the model. This can sometimes present challenges, as many WEC devices conform to an irregular and complex geometry. The difficulty then arises in the effort to construct a domain mesh that can capture the intricacies of the WEC surface topology. In OpenFOAM the modeller may first create a background mesh that encompasses the entire domain. The WEC geometry is created in independent CAD software and the file is stored as an *.STL or *.OBJ file. These are lightweight file formats that describe the structure's surface geometry in the form of vertex coordinates and surface or vertex normals which are obtained when the surface geometry is tessellated into a number of facets during the *.STL or *.OBJ file conversion process. The solid-body position in the CFD domain is determined and the background mesh is chiselled away in order to fit the solid body surface. A cell castellation process is performed to fit the cells to the solid surface. This process only occurs in those cells that contain an edge (in two-dimensional simulations) or surface (in three-dimensional simulations) boundary on the solid body. The castellation process may be iteratively performed to better capture the surface topology. Then, those cells that lie entirely within the volume of the solid body are removed and the cell vertices are snapped to the *.STL or *.OBJ surface geometry. Additional layers of cells can be added along the solid surface boundary to improve the local mesh quality at the WEC surface.

SnappyHexMesh has become a widely used tool for the generation of CFD domain meshes around complex and irregular shaped objects.

Dynamic mesh methods   With the exception of oscillating water columns and overtopping structures, most devices used for extracting wave energy displace due to the wave-structure interaction. When conducting numerical simulations the motion of these devices must be captured accurately. This can sometimes pose a challenge to the stability of simulations. There are three main methods for the implementation of dynamic meshes in CFD simulations:

1. dynamic mesh morphing,

2. sliding interface mesh,

3. overset mesh.

Dynamic mesh morphing is a technique employed to allow for the displacement of a solid body. This technique is usually selected for simulations in which the solid body

displacements are small or those simulations in which a single degree of freedom displacements occur. Grid connectivity is maintained as the solid body displaces. This means that the cell edges connecting the grid nodes remain unchanged. If the displacement of the solid body is excessive the grid may distort excessively resulting in a low-quality mesh with high aspect ratio cells or highly skewed grid cells that will reduce the accuracy of the solution or in extreme cases cause the simulation to fail. This method is seldom used in the simulation of WECs due to the relatively high amplitude, multi-degree of freedom motions to which due to their relatively high amplitude, multi-degree of freedom motions. In the OpenFOAM software, a *sixDoFRigidBody-Motion* solver is included which can manipulate the mesh according to the dynamic mesh morphing method. Using this technique, an inner region must be around the solid displacement body and an outer region some distance away from the body must be defined. These regions are usually defined by a radial distance away from the body. The mesh in both the inner and outer regions does not distort as the solid body displaces, but the mesh in the inner region will deform. In OpenFOAM the mesh displacement in the intermediate region is controlled by the spherical linear interpolation (SLERP) algorithm, based on the distance from the intermediate region cell to the moving body. This algorithm allows the mesh quality to be strictly controlled. The body displacement is diffused into the domain according to the Laplace equation:

$$\nabla \cdot (k \nabla u) = 0, \tag{2.73}$$

where k is the diffusivity coefficient and u is the velocity of the moving body.

The main disadvantage of the mesh morphing method is that solid body displacements should be small and the modeller should have prior knowledge of the amplitudes of displacement before simulations are conducted. Additionally, the outer radius which defines the extent of the mesh distortion for a moving body cannot overlap with another mesh distortion region around a second body. For this reason, this method is not suitable for use in simulations with multiple adjacent displacing bodies. This dynamic mesh modelling technique is especially applicable for simulating the motion of small amplitude heaving buoys.

The sliding interface mesh is an alternative dynamic meshing method that can be used to allow for large displacements of solid bodies in numerical simulations. In this technique, grid connectivity is not maintained. The user defines a background mesh that is applied throughout the domain and a local mesh that is defined in the region of the solid body. The local mesh is allowed to slide or rotate, relative to the background mesh. The interface between the two mesh regions can either be a straight line to allow for a single degree of freedom motion such as heave or it may be a curved interface to allow for rotational motion of the solid body. The solution to the governing equations is computed separately in each of the mesh regions and the field variable data such as pressures or velocities are transferred across the interface using an arbitrary mesh interface (AMI) technique. As the inner mesh region slides relative to the outer mesh region the cells become misaligned at the interfacial boundary the AMI algorithm computes the input weights from each face of the intersecting cells based on the fraction of the overlapping areas at the boundary. For two boundary adjacent cells, the sum of the weights should approach unity in order to preserve simulation stability.

The sliding interface mesh method has some advantages over the mesh morphing technique. The method can process large displacements especially in rotational degrees of freedom. Also since the dynamic mesh region is limited to the area around the moving solid body, this method is more suitable for simulation cases with multiple moving bodies in close proximity. Since the domain meshes in both the inner and outer do not deform, the cells preserve their shape, therefore errors arising for deformed cells are minimised. The most conspicuous disadvantage of the sliding interface mesh method is that this technique is mainly limited to a single degree of freedom motion of the solid body.

The overset grid approach is a powerful technique in dynamic meshing methods. In this method, two independent, disconnected meshes are defined within the domain. The first mesh is a background mesh that is applied throughout the entire domain. The second mesh is a body-fitted mesh that is defined around the WEC solid body and overlays the background mesh. The two meshes are permitted to move relative to each other and neither independent mesh deforms or distorts, keeping its original structure. Using this technique, the shifting cells within the domain (in both the background and overset mesh) are classified according to their characteristics and locations within the domain at each time step. The cells are categorised as blocked cells, fringe cells, donor cells, and acceptor cells. Blocked cells are those cells that are within the volume of the solid body. These are inactive cells, sometimes called hole cells as they form a hole in both the body-fitted and the background mesh. In the background mesh, the fringe cells are those cells that are adjacent to the hole. In the body-fitted mesh, the fringe cells are those cells that are at the outer boundary of the grid. Donor and acceptor cells are those additional cells that are in the region common to both the background and body-fitted meshes. An interpolation process is used to map the boundary values to the fringe cells and interpolation of values is performed between the donor and acceptor cells on both the body-fitted and the background meshes. The main advantage of the overset grid method is that it allows for large motions in multiple degrees of freedom whilst the mesh quality does not degrade. The main disadvantage of the method is that it requires significantly more processing time due to the computationally demanding interpolation procedure.

2.3.4.3 Boundary and initial conditions

In order to reduce the number of unknown terms in the system of governing equations, boundary conditions are specified at the edges of the fluid domain. There are a great number of disparate boundary conditions to simulate different physical circumstances. It is beyond the scope of this text to investigate all of these boundary conditions individually, but it is of critical importance that the CFD user is familiar with the physical significance and the mathematical implementation of the boundary conditions that are specified at any domain boundary. Most commonly-used boundary conditions in the case of wave energy harvesting include no-slip boundaries at solid surface boundaries or wave absorption boundary conditions at domain edges to prevent wave reflection. Additionally, initial conditions are specified either at a boundary edge or internally at some location within the domain. For the purpose of

modelling wave energy harvesting systems, these initial conditions usually consist of some form of wave generation condition at one or more boundary edges.

2.4 WAVE TANK EXPERIMENTS

Numerical solvers, as described in earlier sections, are very useful to model wave-structure interaction problems in various conditions, in particular in the stages of WEC development. To gain trust in the simulations and to capture physical effects accurately, numerical solvers need to be complemented by physical experiments. With the increase in TRL of the WECs, wave tank experiments on the scaled physical model are required to gain confidence in the WEC's performance in a controlled, repeatable, and high-fidelity laboratory environment, prior to sea trials that are uncontrollable, uncertain, and both time- and cost-consuming.

2.4.1 Objectives

The objectives of wave tank experiments vary with the TRL of the WEC. For WECs at an early stage of development with low TRL (e.g., TRL≤4), wave tank experiments are used to evaluate their power absorption performance, PTO control strategies, and numerical models of wave-structure interaction in typical operational sea states. The evaluation outcomes support further design optimisation of the WECs at the early conceptual stage where design flexibility is high. For mature WEC technologies with higher TRL (e.g., TRL≥5), wave tank experiments can be used to assess their hydrodynamic responses, structural and mooring forces, and PTO efficiency, loads, and reliability in operational and extreme sea states at particular sea sites. Such assessments aim to further improve soundness in the engineering solutions and de-risk the subsequent sea trials.

2.4.2 Wave generation

Making desired and repeatable waves is fundamental to wave tank experiments. There are two main, different types of wavemakers used at the wave tank, according to the water depth of the experiments.

Piston wavemakers are used to simulate shallow water scenarios, where the water depth is roughly smaller than half a wavelength. Here the orbital particle motion is compressed into an ellipse and there is significant horizontal motion on the floor of the tank. This type of paddle is used to generate waves for modelling coastal structures, harbours, and shore-mounted wave energy devices.

Flap paddles are used to produce deep water waves where the orbital particle motion decays exponentially with depth and there is negligible motion at the bottom. Typical applications are the modelling of floating structures in deep water and the investigation of the physics of ocean waves. Often the hinge of the paddle is mounted on a ledge some distance above the tank floor.

To generate the desired wave spectra $S_{\eta d}(\omega)$, the property function $T(\omega)$ of the wavemaker should be confirmed, which is determined by mechanical transfer function $T_1(\omega)$, hydrodynamic transfer function $T_2(\omega)$, and deformation function of the wave

$T_3(\omega)$. $T_1(\omega) = e/R(\omega)$ is the transfer function between the analogue voltage $R(\omega)$ and paddle position e, $T_2(\omega, h) = A_0/e$ is the transfer function between the paddle position e and wave amplitude A_0, and $T_3(\omega)$ is the function of the wave deformation along the wave tank, determined by the wave conditions, water depth, and the boundary conditions. Thus, the transfer function of the wavemaker system $T(\omega)$ (unit: m/V) is given as follows:

$$T(\omega) = T_1(\omega)T_2(\omega, h)T_3(\omega). \tag{2.74}$$

For the piston type wavemaker $T_2(\omega, h)$ is given by [856]:

$$T_2(\omega, h) = \frac{4\sinh^2 kh}{2kh + \sinh 2kh}. \tag{2.75}$$

For the flap type wavemaker $T_2(\omega, h)$ is given by [856]:

$$T_2(\omega, h) = \frac{4\sinh kh}{kh}\left(\frac{1 - \cosh kh + kh\sinh kh}{2kh + \sinh 2kh}\right). \tag{2.76}$$

Thus, the spectral of wave maker is given by:

$$S_V(\omega) = \frac{S_{\eta d}(\omega)}{|T(\omega)|^2}. \tag{2.77}$$

The voltage signal of the wave maker can be obtained from a spectral analysis of the generated wave. In another word, the time signal of the wave can be represented as a superposition of a series of sinusoidal waves, and thus the voltage signal of the wave maker is [856]:

$$V(n\Delta t) = \sum_{i=1}^{M} \sqrt{2S_V(\hat{\omega}_i)\Delta\omega_i}\cos(\hat{\omega}_i n\Delta t + \beta_i) \tag{2.78}$$

where $V(n\Delta t)$ has the unit volt (V), and $n\Delta t(n = 0, 1, 2...)$ is the temporal discrete points.

2.4.3 Wave tank dimensions

The width of the tank depends on the proposed model tests. 2D model tests are usually carried out in a narrow straightforward wave tank, i.e., a wave flume, with the model fully blocking the width of the flume. The wave flume wall is usually transparent to enable good visibility of the wave-structure interaction. This type of model is relatively easy to analyse as the waves and flow act in a plane. For 3D model tests, a wider wave tank is needed so that the waves can pass around the model's sides. Generally, the most realistic mixed sea waves have to be modelled in a wide tank with multiple, individually-controlled paddles. A full range of waves and wave spectra can be generated by software controlling the paddles.

The wave tank is divided into three distinct zones (see Figure 2.6) and each zone should be sufficiently long. Firstly, there is a paddle and enough space for the evanescent waves to decay. Waves from a well-controlled paddle need to travel approximately

twice the hinge depth of the paddle to become fully developed. Secondly, the model zone depends on the size and motion of the model. Enough length is needed in this zone to guarantee the sample time and avoid the influence of the reflected wave from the paddle. For wide tanks, the combination of width and length determines the angle of the waves that approach the model. Thirdly, there is the wave absorbing beach, which has to be at least half the length of the design wavelength to achieve 90% absorption.

The depth of the wave tank depends on the experimental water depth. Sufficient depth in the wave tank is needed to generate the desired wave conditions and the reflected phenomenon should also be considered to avoid the top overflow. The wave characters depend highly on the water depth. The relationship between the water depth and wave nonlinearity can be seen in Figure 2.3. For experiments using optical equipment (especially for this device to be located at the side of the wave tank), the depth of the wave tank is a very important factor to be considered since most wave tanks have steel beams. A wave tank with proper depth and width can avoid any beam sheltering of the model.
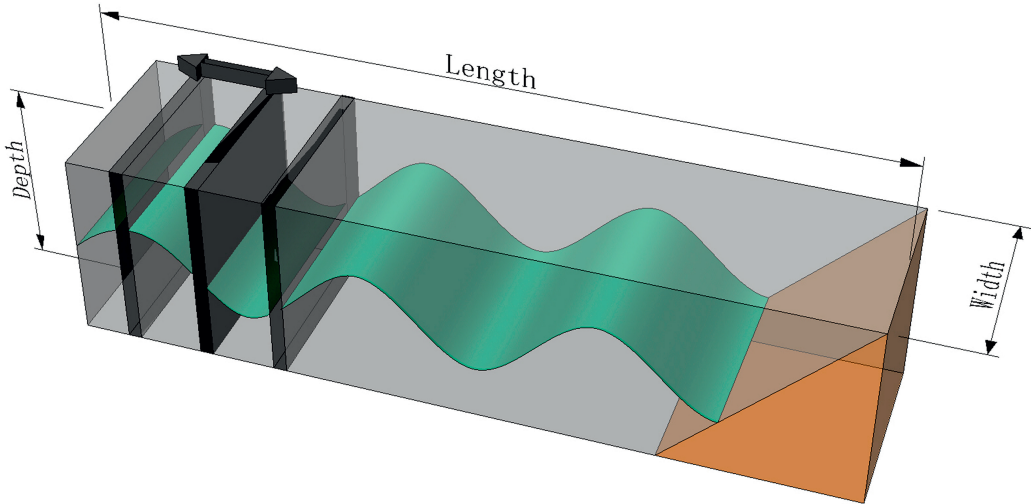

Figure 2.6: Schematic of wave tank

2.4.4   Scaling

Nearly all physical modelling of WECs is conducted at scale. A properly-scaled physical model is expected to behave in a manner similar to the prototype it is intended to emulate. To relate the responses of a scaled model with the prototype, the scaling laws or principles of similitude are considered.

2.4.4.1   *Scaling law*

Geometric similarity, kinematic similarity, and dynamic similarity are the three basic principles of similarity that should be taken into account for the study of fluid-structure interaction. After applying these three principles of similitude to a WEC

problem, six relevant non-dimensional numbers, i.e., the *Froude*, *Reynolds*, *Cauchy*, *Weber*, *Euler*, and *Strouhal* numbers [306], can be obtained, of which the first four represent the ratio of the inertial forces to the gravity, viscous, elastic, and surface tension forces, respectively; whilst the Euler number corresponds to the ratio of the pressure forces to the inertial forces, and the Strouhal number is associated with the ratio of the temporal inertial forces to the convective inertia forces. To achieve complete similitude, all six of these criteria should be met, which is, however, not possible unless the scale factor is 1.0, i.e., the model is not scaled.

When testing WECs at scale, a decision over which criterion to uphold must be made. As inertial and gravitational forces are normally predominant for the scaling of wave interactions with WECs, most WEC tests are scaled following Froude's scaling law, which can be given by:

$$F_r = \frac{U}{\sqrt{gl}}, \tag{2.79}$$

where U is the fluid velocity, g the gravitational acceleration, and l the characteristic length.

Table 2.2 presents more explicitly the direct application of Froude's scaling law for the scaled model-related characteristics and results. The term *power density* refers to the power per unit length.

2.4.4.2 Scale issues

For some special circumstances, it may be necessary to use distorted models in the framework of Froude's scaling law. For example, when modelling a WEC floating in deep water, the horizontal lengths may be tens of m long, while the water depth may be hundreds of m. To model this system in a laboratory requires a horizontal scale large enough to avoid significant surface tension effects, and a vertical scale factor small enough to fit the model into the available space.

For some WECs, different parts of the model could be associated with different scaling laws. For example, the power take-off mechanism of oscillating water column (OWC) devices relies on the aerodynamics as the air in the OWC chamber is forced back and forth through a turbine. The hydrodynamics and aerodynamics of the OWC model are relevant to the Froude and the Reynolds laws, respectively, and their combination makes the scaling considerations for OWCs more complex than standard Froude's scaling law. More information on the topic of OWC scaling can be found in [823].

2.5 MODELLING OF INTERACTION BETWEEN OCEAN WAVE AND WAVE ENERGY CONVERTER

Complementary to costly model-scale experiments, numerical modelling is often used to understand the performance of the wave energy converter. The majority of studies on wave energy conversion have used linear potential flow theory as the basis for modelling hydrodynamics arising from wave-body interaction [622], as discussed earlier in this chapter. Although this simplifies/linearises the wave-structure interaction

Table 2.2: Scale factors for the Froude's scaling law.

Quantity	Dimension	Scale factor
Wave height/length	[L]	C_l
Wave period	[T]	$C_l^{0.5}$
Wave frequency	$[T^{-1}]$	$C_l^{-0.5}$
Power density	$[MLT^{-3}]$	$C_l^{2.5}$
Power	$[ML^2T^{-3}]$	$C_l^{3.5}$
Energy	$[ML^2T^{-2}]$	C_l^4
Linear displacement	[L]	C_l
Angular displacement	[-]	1
Linear velocity	$[LT^{-1}]$	$C_l^{0.5}$
Angular velocity	$[T^{-1}]$	$C_l^{-0.5}$
Linear acceleration	$[LT^{-2}]$	1
Angular acceleration	$[T^{-2}]$	C_l^{-1}
Mass	[M]	C_l^3
Volume	$[L^3]$	C_l^3
Pressure	$[ML^{-1}T^{-2}]$	C_l
Force	$[MLT^{-2}]$	C_l^3
Torque	$[ML^2T^{-2}]$	C_l^4
Linear stiffness	$[MT^{-2}]$	C_l^2
Angular stiffness	$[ML^2T^{-2}]$	C_l^4
Linear damping	$[MT^{-1}]$	$C_l^{2.5}$
Angular damping	$[ML^2T^{-1}]$	$C_l^{4.5}$

problem, as well as speeding up the simulation process, the utilisation of a linear solver (which assumes that the wave steepness and body motion are both small) usually contradicts the large motion arising from the wave energy converter and thus does not ensure the fidelity of the simulation results in medium to large wave conditions. As shown in Figure 2.3, deep-water waves with a steepness less than 0.01 can be approximated by a sinusoidal wave by applying linear wave theory [248]. However, wave energy converters are usually located in either intermediate water or shallow water, where waves are usually described by Stokes's wave theory or cnoidal wave theory. The operational conditions of WECs exceed the limits of linear wave theory and cover Stokes waves of the 2nd and 3rd orders [620]. At the extreme opposite, the

Navier-Stokes equation based CFD methods capture the full nonlinear hydrodynamics in the wave-body interaction problem leading to high fidelity simulation results regardless of the system's operational conditions. However, CFD is often only used to assess the survivability of the device, due to its high computational requirement.

A compromise between the linear method and the Navier-Stokes solver also exists [620], often termed weakly nonlinear solvers. These solvers are built based on the potential flow theory but with weak nonlinearities augmented to consider additional nonlinear effects. Examples for these nonlinearities are the consideration of the instantaneous body position in the wave field, extrapolation of wave kinematics above the mean sea level, and consideration of quadratic transfer functions for second-order wave-excitation forces. The computational time requirements for these codes are usually higher than for the purely linear codes, but they are often less expensive than CFD, whilst still able to capture notable nonlinearities. A typical example of a weakly nonlinear solver is the weak-scatterer potential flow method proposed for the seakeeping analysis of ships with forward speed [613], which is formulated based on the assumption that the perturbation wave field generated by the body oscillation is small compared with the incident wave field, such as the free surface conditions can be linearised at the incident wave elevation level. The weak-scatterer method takes into account the unsteady and nonlinear hydrodynamic loads associated with dynamic wave-body interactions. A further simplified version of the weak-scatterer method is the body-exact potential method, which assumes the free surface conditions can be linearised around the mean free surface elevation. This solver was proposed to account for the body motion induced nonlinearities but is only valid when small steepness waves are present. It is a compromise between the weak-scatterer method and the linear method. Table 2.3 summarises the main differences between the linear method, body-exact solver, weak-scatterer solver, and CFD [178]. Despite the fact that a large number of weakly nonlinear solvers have been proposed for WEC investigations, their capabilities in capturing nonlinearities arising from wave-WEC interactions in various wave conditions remain questionable. The WEC research and development community lacks and urgently needs a universal high-fidelity but low-cost model to improve confidence levels in numerical predictions of power production and load estimates, which are important quantities for the development of reliable and cost-efficient WECs.

To gain confidence in using numerical models and assessing the accuracy of these codes, the International Energy Agency Ocean Energy Systems (IEA OES) Task 10 project [830] compared a large number of linear, weakly nonlinear, and highly nonlinear codes on a simple WEC system of a heaving buoy. The main outcome of this project demonstrated that, in steep waves, the weakly nonlinear codes are able to capture higher-order peaks in the WEC response because of the consideration of nonlinear hydrostatics and Froude-Krylov forcing, and therefore they predict a reduced mean power output of the WEC that is closer to the reality. Highly accurate experiments were carried out on a heave decay test for a sphere [419], whose results were compared with the linear potential flow, nonlinear potential flow, and RANS CFD methods. For low drop heights, all methods performed very well, with deviations less than 1 mm for all models, but for larger drop heights and applications

Table 2.3: Main differences between the four wave-body interaction modelling methods. See [178] for more details.

	Linear potential flow	**Body-exact potential flow solver**	**Weak-scatterer potential solver**	**Navier-Stokes-based CFD solver**
Assumption	$\begin{cases}\text{Irrotational and}\\\text{inviscid fluid,}\\\text{small body motion,}\\\epsilon \ll 1\end{cases}$	$\begin{cases}\text{Irrotational and}\\\text{inviscid fluid,}\\\epsilon \ll 1\end{cases}$	$\begin{cases}\text{Irrotational and}\\\text{inviscid fluid,}\\\Phi_P = \mathcal{O}(\Phi_I)\end{cases}$	Isotropic fluid
Hydrodynamics decomposition	$\Phi = \Phi_I + \Phi_S + \Phi_R$	$\Phi = \Phi_I + \Phi_P$		N/A
Meshed free surface	$z = 0$		$z = \eta_I(x,y,t)$	$z = \eta(x,y,t)$
Meshed body surface	$S(0)$	$S(t)$		
Hydrodynamic force computation	Sum of excitation and radiation forces	Integration of total pressure over the wetted body surface		Integration of total stress over the wetted body surface
Fluid vortices	NO			YES
Wave breaking	NO			YES
Drag force	NO, a Morison equation (as detailed in Section 3.1) can be added			YES
Surface piercing	NO	YES		
Computational speed	Extremely fast	Medium	Slow	Extremely slow

with large motion amplitudes, the potential flow methods should be used with care; whereas the RANS models, if proper convergence is reached, are capable of producing accurate results for all drop heights. In the Collaborative Computational Project in Wave Structure Interaction (CCP-WSI), numerical results are compared without prior access to experimental data in a blind test approach [653]. The project has been conducted via several steps with increasing complexity, and has considered interactions between focused waves and structures. It was concluded that Navier-Stokes solvers and hybrid methods were superior to linearised methods under these extreme wave conditions; however, heave motion was predicted reasonably well by all methods.